Optical band gap in a cholesteric elastomer doped by metallic nanospheres

Julio C. Hernández and J. Adrián Reyes*
Instituto de Física, Universidad Nacional Autónoma de México, Apartado Postal 20 364 01000, México City, Mexico
(Received 17 February 2017; published 11 December 2017)

We analyzed the optical band gaps for axially propagating electromagnetic waves throughout a metallic doped cholesteric elastomer. The composed medium is made of metallic nanospheres (silver) randomly dispersed in a cholesteric elastomer liquid crystal whose dielectric properties can be represented by a resonant effective uniaxial tensor. We found that the band gap properties of the periodic system greatly depend on the volume fraction of nanoparticles in the cholesteric elastomer. In particular, we observed a displacement of the reflection band for quite small fraction volumes whereas for larger values of this fraction there appears a secondary band in the higher frequency region. We also have calculated the transmittance and reflectance spectra for our system. These calculations verify the mentioned band structure and provide additional information about the polarization features of the radiation.

DOI: 10.1103/PhysRevE.96.062701

I. INTRODUCTION

The Bragg phenomenon is displayed by a slab of a dielectric material whose electromagnetic properties are changing periodically in the thickness direction. Its main feature is a very high reflectance for a given wavelength interval, on the condition the slab is thick enough to have a sufficient number of periods. This behavior has been widely applied to make dielectric mirrors in optics [1]. Periodicity is provided by structural chirality which implies a helicoidal variation of anisotropy along a certain direction. Some examples of structurally chiral materials are cholesteric liquid crystals [2,3] and chiral sculptured thin films [4]. For these media, when incident electromagnetic plane waves of left- and right-circular polarization states are reflected and transmitted differently in the Bragg wavelength regime, the Bragg phenomenon is then called the circular Bragg phenomenon (CBP). Exhibition of the CBP by cholesteric liquid crystals and chiral sculptured thin films guarantees their use as circular-polarization rejection filters in optics [2,4]. Control of the CBP is quite useful for tuning the Bragg regime as well as for switching applications. One way would be to use structurally chiral materials that are electro-optically controlled systems. This possibility, also suggested by the fabrication of electro-optic filters [5], was proposed and theoretically examined [6]. Cholesteric elastomers are formed by monomers of liquid crystals cross linked to polymeric chains; this union produces a flexible material whose molecular order is similar to cholesteric liquid crystals with the advantage that in this new material it is possible to change the optical properties by means of macroscopic deformations [7]. The interest in the optical properties of these materials has recently increased due to the attainment succeeded by Kim and Finkelmann who developed a method to create monodomain nematic and cholesteric elastomers [8]. Even more, a more affordable procedure to produce slabs of cholesteric elastomers by cross linking under UV irradiation has been subsequently established [9]. For normally incident light on a contracted cholesteric sample, a blue-shift of the photonic stop band has been experimentally and theoretically obtained [10]. A numerical study of the circularly polarized reflectances due to an elastomer slab elongated by the influence of a uniaxial transverse strain was done [11]. Nested optical band gaps were found for left- and right-circularly polarized light.

A different option to handle the band structure of photonic crystals is by means of contaminating them with materials possessing sharp optical resonances. This remarkably large resonance has been evinced for a nanocomposite consisting of metallic nanoballs randomly dispersed in a transparent matrix, whereas the optical properties of host materials lack resonant properties [12,13]. Moreover, many periodic chiral dielectric [14] and metallic [15] structures have attracted important consideration since some years because of its capability to provide giant circular dichroism [14] or giant gyrotropy [15], even for the optical regime. Nowadays, chiral dielectric structures surpass the functioning of chiral metallic structures by a large margin regarding their losses. Moreover, various works have demonstrated that the photonic band gap can be significantly distorted by inserting metallic dispersive inclusions [16]. For instance, a graphene photonic band structure can be tailored by including metallic sheets [17]. Also, a system owing a nonchiral band gap for which gold helices have been inserted can act as a circular polarizer of the same handedness of the helices [18]. Also, Lakhtakia *et al.* has theoretically examined the effect of metal nanospheres embedded in a medium which is the solid analog of a chiral smectic liquid crystal. They have found that even for a quite small filling factor, a meaningful red-shift was obtained [19].

As in many of the above-mentioned works, we use an effective permittivity theory to characterize the nanocomposite showing that the dielectric resonance of the whole structure is due to the plasmon resonance of nanoparticles. Their effective permittivity can be in excess up to 10 in comparison with the same material without the small inclusions. Hence, dispersion of resonant medium combined with the dispersion of helicoidal structures provides a different tool to manipulate the circular Bragg phenomenon.

Our research is aimed to study the band gap of a cholesteric elastomer with metallic nanoparticles dispersed inside it, subjected to an externally imposed deformation for tuning the circular Bragg regime exhibited by the elastomer in the absence of the strain. In Sec. II we discuss the elastic model

*Corresponding author: adrian@fisica.unam.mx

for describing a cholesteric elastomer slab subjected to a mechanical strain applied along the helix axis of the elastomer. Section III contains a brief description of the optical permittivity matrix of a chiral material. Also, in this section the effective permittivity tensor of the composite structure is obtained and the Oseen transformation is employed to derive an analytical expression for the band reflection in the Bragg regime. Section IV accounts for the numerical results and discussions.

II. ELASTIC ELASTOMER ENERGY

We start by assuming a monodomain cholesteric elastomer submitted to a longitudinal elongation. The microscopic statistical-mechanical theory of rubber elasticity [7] allows to derive the classical nematic rubber elasticity energy density so called the trace formula when anisotropy is taken into account. It is given by

$$F = \tfrac{1}{2}\mu \,\mathrm{Tr}[\tilde{l}_0 \cdot \tilde{\eta}^T \cdot \tilde{l}^{-1} \cdot \tilde{\eta}], \tag{1}$$

where $\mu = n_s \kappa_B T$ is the rubber shear modulus, here Tr denotes the trace of the tensor, and the local step-length tensors for a locally uniaxial medium are

$$\tilde{l}_0 = \tilde{I} + (r-1)\hat{\mathbf{n}}_0\hat{\mathbf{n}}_0, \tag{2}$$

$$\tilde{l}^{-1} = \tilde{I} + (1/r-1)\hat{\mathbf{n}}\hat{\mathbf{n}}, \tag{3}$$

where r is the anisotropy ratio and $\tilde{I}$ is the identity tensor.

In deducing Eq. (1), the entanglements, finite extensibility, and semisoftness have been neglected. Here, the director corresponding to the initial configuration is written as

$$\hat{\mathbf{n}}_0 = (\cos\phi_0, \sin\phi_0, 0), \tag{4}$$

where the angle $\phi_0 = q_0 z$ has a helix wave number $q_o = 2\pi/p$ and a spatial periodicity or pitch p. This is determined by the concentration and the helical twisting power [20] of the chiral constituents. Usually, the pitch is of the same order as the wavelength. After the distortion, the director is aligned along the surface of a cone, which can be described by

$$\hat{\mathbf{n}} = (\sin\alpha\cos qz, \sin\alpha\sin qz, \cos\alpha), \tag{5}$$

where α is the azimuthal angle.

When the elastomer is elongated, a selected chain's end-to-end vector $\mathbf{R}$ will stretch proportionally to the body's strain. The proportionality factor is given by the deformation tensor $\tilde{\eta}$ which in the case of an expansion parallel to the helix axis $\mathbf{z}$, $\tilde{\eta}$ is given by [7]

$$\tilde{\eta} = \begin{pmatrix} \frac{1}{\sqrt{\eta}} & 0 & \eta_{xz}(z) \\ 0 & \frac{1}{\sqrt{\eta}} & \eta_{yz}(z) \\ 0 & 0 & \eta \end{pmatrix}, \tag{6}$$

where we have set $\eta_{zz} = \eta$. The fact that $\mathrm{Det}(\tilde{\eta}) = 1$ ensures that the distortions described by this expression keep fixed the body volume. There is no compatibility inconsistency due to the z dependence of the elongations $\eta_{xz}(z)$ and $\eta_{yz}(z)$. In contrast, the z dependence of their conjugate strains $\eta_{zx}(z)$ and $\eta_{zy}(z)$ would lead to compatibility mismatch as, for instance, the expression $\partial\eta_{zx}(z)/\partial z = \partial\eta_{zz}(z)/\partial x$ cannot be fulfilled unless we set $\partial\eta_{zx}(z)/\partial z = 0$. Finally, η_{xy} and η_{yx} could exist but numerical tests [21] suggest that it is not possible. The two shear strains η_{xz} and η_{yz} should be proportional to each other so that they are part of a shear in the plane of $\hat{\mathbf{n}}_0$ and $\hat{\mathbf{n}}$. These two shears help to accommodate the rotation of the chain distributions by keeping the elastic energy low, while the director $\hat{\mathbf{n}}$ rotates. *That is, the network deforms to allow rotate* $\hat{\mathbf{n}}$ *practically without investing energy.* All physical dimensions in the stretched system are supposed to scale by the affine strain as $z \to z/\eta$ which leads to the associated expansion of the cholesteric pitch $q = \frac{q_o}{\eta}$.

From the above expressions, the free energy for an elastomer under mechanical strain is derived. Hence, we minimize the free Helmholtz energy first with respect to the strains η_{xz} and η_{yz} and then with respect to χ, where $\chi = \frac{\pi}{2} - \alpha$, to get

$$\chi(\eta) = \arcsin\sqrt{\frac{\eta^{3/2}-1}{r-1}}. \tag{7}$$

Notice from this expression that the nematic's vector is totally aligned with the z axis when the critical longitudinal stress reaches the value

$$\eta_M = r^{2/3}, \tag{8}$$

where η is restrain to the interval $1 \leqslant \eta \leqslant \eta_M$ *because a uniaxial compression* ($\eta < 1$) *parallel to the helix axis leaves the helical structure invariant and, an extension beyond* η_M *does not change any more* χ (see Fig. 1).

Equation (7) gives an expression for the director vector $\hat{\mathbf{n}}$ from which we find the local relative permittivity tensor of the elastomer:

$$\tilde{\epsilon} = \epsilon_\perp \tilde{I} + \epsilon_a \hat{\mathbf{n}}\hat{\mathbf{n}}, \tag{9}$$

where $\epsilon_a = \epsilon_\parallel - \epsilon_\perp$ is the local relative permittivity anisotropy, $\epsilon_\parallel$ and $\epsilon_\perp$ are the local relative permittivities parallel and perpendicular to the director $\hat{\mathbf{n}}$. It is wealth to mention that the only dependence of $\tilde{\epsilon}$ on the deformation tensor is on $\hat{\mathbf{n}}$ because the main effect of stretching the elastomer in the given interval of η is to rotate the mesogenic molecules which remained chemically attached to the polymer backbone [7].

III. ELECTROMAGNETIC PROPAGATION

Faraday and Ampere-Maxwell equations without sources in SI units are given by

$$\nabla \times \mathbf{E} = i\omega\mu_o \mathbf{H}, \tag{10}$$

$$\nabla \times \mathbf{H} = -i\epsilon_o \omega \tilde{\epsilon}(z) \cdot \mathbf{E}, \tag{11}$$

where the z-dependent local relative permittivity tensor of the elastomer, submitted to an axial stress, was determined in Sec. II. The normal incidence solutions for the above equations can be written as

$$\mathbf{E}(\mathbf{r}) = \mathbf{e}(z), \tag{12}$$

$$\mathbf{H}(\mathbf{r}) = \mathbf{h}(z), \tag{13}$$

where ω is the wave frequency, $\mathbf{e}(z) = (e_x(z), e_y(z), e_z(z))$ and $\mathbf{h}(z) = (h_x(z)\ , h_y(z), h_z(z))$ are electric and magnetic amplitudes in the elastomer slab.

Upon substituting Eqs. (12) and (13) into Maxwell equations we find a set of equations which only depend on z.

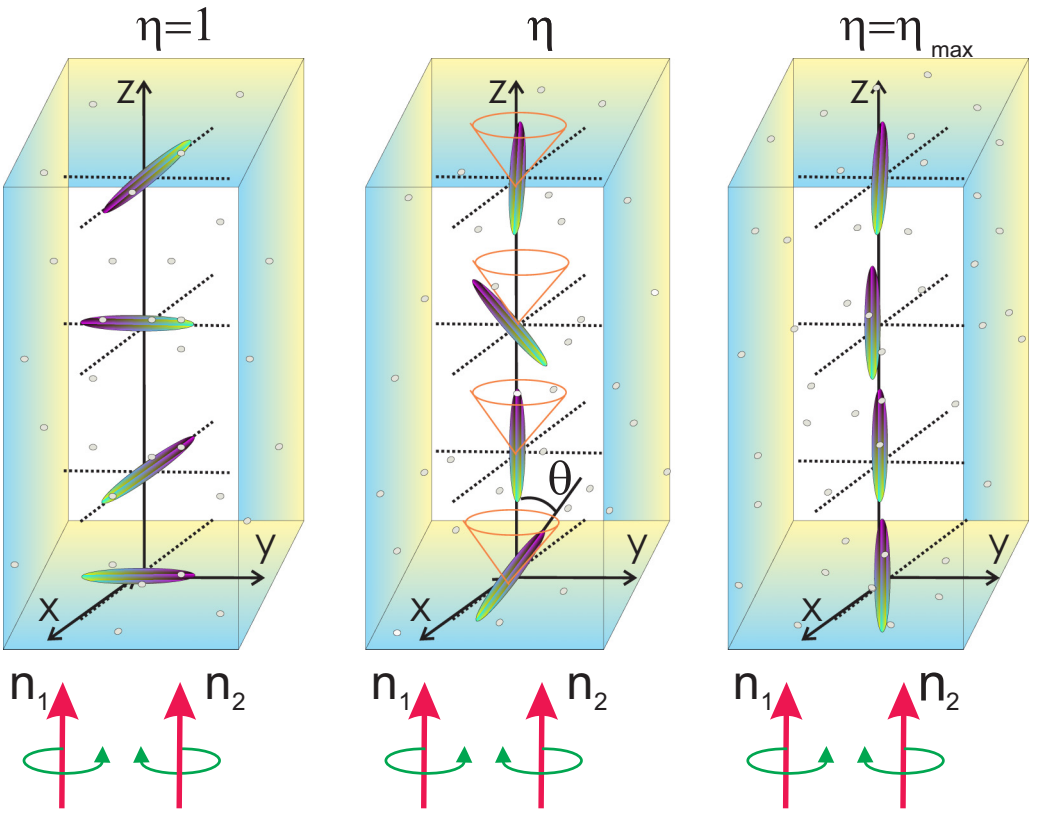

FIG. 1. Schematic of the system.

We solve them for $e_z(z)$ and $h_z(z)$ in terms of the remaining components to obtain a system only for the transverse components of the fields which can be written as the matrix first order equation [22]

$$\frac{d}{dz}\mathbf{v}(z) = -i\tilde{M}(z)\cdot\mathbf{v}(z), \tag{14}$$

where

$$\mathbf{v}(z) = \begin{pmatrix} e_x(z) \\ e_y(z) \\ h_x(z) \\ h_y(z) \end{pmatrix}. \tag{15}$$

Here, the 4×4 matrix is defined as

$$\tilde{M}(z) = \begin{pmatrix} 0 & 0 & 0 & \beta \\ 0 & 0 & -\beta & 0 \\ \frac{\epsilon_{yz}\epsilon_{zx}\zeta}{\epsilon_{zz}} - \epsilon_{yx}\zeta & -\epsilon_{yy}\zeta + \frac{\epsilon_{yz}\epsilon_{zy}\zeta}{\epsilon_{zz}} & 0 & 0 \\ \epsilon_{xx}\zeta & \epsilon_{xy}\zeta - \frac{\epsilon_{xz}\epsilon_{zy}\zeta}{\epsilon_{zz}} & 0 & 0 \end{pmatrix}, \tag{16}$$

where ϵ_{mn} $(n,m = 1,2,3)$ represent the elements of the local relative permittivity tensor $\tilde{\epsilon}$, $\zeta = \epsilon_o\omega$, and $\beta = \mu_o\omega$.

A. Effective permittivity of a dielectric matrix with metallic inclusions

The effective permittivity of a dielectric matrix isotropic medium containing a quite small volume fraction of randomly dispersed inclusions can be calculated by using the Maxwell-Garnett formula [12,23–25] which was obtained by assuming the quasistatic approximation. Its main features are (i) the mixture is electrodynamically isotropic, (ii) the mixture is linear, that is, none of its constitutive parameters depend on the intensity of electromagnetic field, (iii) the parameters of the mixture do not change in time as a result of external forces, (iv) the characteristic size of inclusions is small compared to the wavelength of light in the effective medium, (v) particles are randomly dispersed and oriented ellipsoids, and (vi) the filling factor should be lower than the percolation threshold, which means that below this threshold there is no formation of long-range connectivity among constituents. The generalization of the Maxwell-Garnett formula for a a locally uniaxial medium has been developed [26]. A general formalism for calculating the effective relative permittivity and permeability tensors has been provided when both the inclusions and matrix media are uniaxial. In the general case, it is necessary to calculate both of them simultaneously, however, the dielectric effective tensor can be greatly reduced in the particular case when we neglect contributions up to third order in the dielectric anisotropy $O[(\epsilon_3 - \epsilon_1)^3]$ of the host medium while keeping an isotropic contaminant and a quite small filling factor f $(f \ll 1)$. In such a limit, the local effective permittivities are [27]

$$\epsilon_\perp^e(\omega) = \epsilon_\perp\left[1 + \frac{f}{\epsilon_\perp/[\epsilon_m(\omega) - \epsilon_\perp] + (1-f)/3}\right] \tag{17}$$

and

$$\epsilon_\parallel^e(\omega) = \epsilon_\parallel\left[1 + \frac{f}{\epsilon_\parallel/[\epsilon_m(\omega) - \epsilon_\parallel] + (1-f)/3}\right], \tag{18}$$

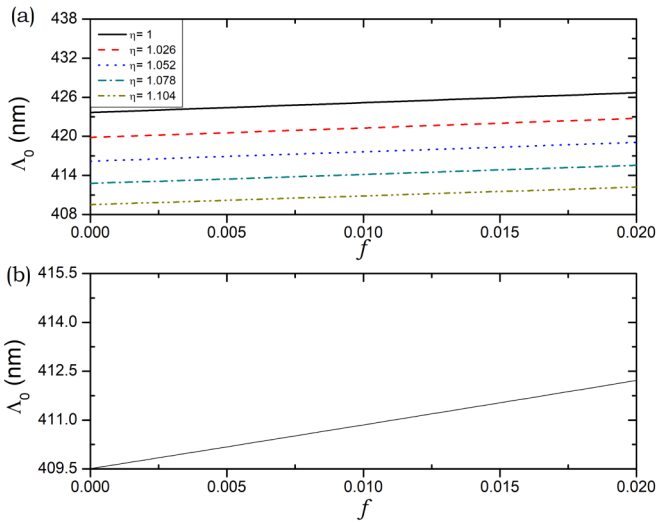

FIG. 2. Resonance wavelength of the relative permittivities (a) ϵ_d and (b) $\epsilon_\perp^e$ versus filling factor parametrized for various values of the deformation parameter.

where $\epsilon_\parallel$ and $\epsilon_\perp$ are the local relative permittivities parallel and perpendicular of the dielectric matrix or host material, and $\epsilon_m(\omega)$ is the local relative permittivity of the metallic particles or guest medium. It is well to stress that this formalism yields physically implausible results when the volumetric fraction of the metal is significantly high in a two-constituent composite material [28,29]. However, that implausibility is not a significant issue in the present context because f of the metal is not expected to exceed 0.02.

We assume in addition the Drude model for a metallic material which provides us an approximation for the permittivity of the nanoparticles. It is written as

$$\epsilon_m(\omega) = \varepsilon_0 - \frac{\omega_p^2}{\omega(\omega + i\gamma)}, \tag{19}$$

with ε_0 the background dielectric constant taking into account contributions from interband transitions, ω_p the plasma frequency, γ the plasma relaxation rate, and, as said above, ω is the frequency of the propagating wave.

Notice that expressions (17) and (18) show a resonant frequency at (neglecting small factor γ^2)

$$\omega_0 = \omega_p \left(\frac{1-f}{3\epsilon_h + (1-f)(\epsilon_0 - \epsilon_h)} \right)^{1/2}, \tag{20}$$

where ϵ_h is a local relative permittivity of the host material ($\epsilon_\parallel$ or $\epsilon_\perp$), notice that ω_0 depends on the primary dielectric properties and the filling factor. A straightforward analysis of (20) demonstrates that, for fixed ϵ_0 and ϵ_h, the resonant frequency ω_0 shifts towards the long-wavelength regime as the fraction of nanoinclusions f increases. In Fig. 2, we depict the associated resonance wavelength $\Lambda_0 = 2\pi c/\omega_0$ as shown for (a) ϵ_d and (b) $\epsilon_\perp^e$ against the filling factor for various values of the deformation parameter η. We have assumed silver nanoballs inclusion with $\varepsilon_0 = 5$ and $\omega_p = 1.367 \times 10^{16}$ Hz. This plot clearly exhibits that Λ_0 increases as a function of f and diminishes as the elastomer is stretched. Hence, we can tune the properties of the band structure by varying these parameters.

B. Effective relative permittivity tensor of a doped elastomer cholesteric

Expressions (9), (17), and (18) can be used to state the effective relative dielectric tensor of the combined structure studied here. Indeed, because the nanoparticles are randomly dispersed in the whole structurally chiral material, the effect on the dielectric properties is to have local effective permittivities $\epsilon_\parallel^e$ and $\epsilon_\perp^e$ that depend on the propagation frequency ω accordingly to Eqs. (17) and (18). Thus, the expression for the effective relative permittivity tensor for a cholesteric elastomer is completely analogous to (9) with the local effective permittivities given by Eqs. (17) and (18):

$$\tilde{\epsilon}^{eff} = \epsilon_\perp^e(\omega)\tilde{I} + [\epsilon_\parallel^e(\omega) - \epsilon_\perp^e(\omega)]\hat{\mathbf{n}}\hat{\mathbf{n}}. \tag{21}$$

Substitution of each element of this effective relative permittivity tensor into Eq. (14) provides the set of differential equations that satisfies the four transversal components of electromagnetic wave field. Notice that, in this case, there are two resonant frequencies due to the two different local effective permittivities.

C. Oseen transformation

The differential system given by Eq. (14) can be solved using a numerical integration. Nevertheless, it is possible to find a reference system, for a normally incident wave, for which the solution can be obtained analytically. Using the Oseen transformation [30], where the reference system rotates along the z axis in the same way as the director $\hat{\mathbf{n}}$.

Let us define a new vector as

$$\mathbf{v}'(z) = \tilde{G}(z) \cdot \Psi(z), \tag{22}$$

where

$$\tilde{G}(z) = \begin{pmatrix} \cos qz & \sin qz & 0 & 0 \\ -\sin qz & \cos qz & 0 & 0 \\ 0 & 0 & \cos qz & \sin qz \\ 0 & 0 & -\sin qz & \cos qz \end{pmatrix}. \tag{23}$$

Substituting the above equation into the differential system Eq. (14), we obtain

$$\frac{d}{dz}\mathbf{v}'(z) = -i\tilde{M}' \cdot \mathbf{v}'(z), \tag{24}$$

with

$$\tilde{M}'(z) = \begin{pmatrix} 0 & iq & 0 & \beta \\ -iq & 0 & -\beta & 0 \\ 0 & -\zeta\epsilon_\perp^e & 0 & iq \\ \zeta\epsilon_d(\eta) & 0 & -iq & 0 \end{pmatrix}, \tag{25}$$

where we have introduced the notation

$$\epsilon_d(\eta) = \frac{\epsilon_\perp^e \epsilon_\parallel^e}{\epsilon_\perp^e \cos^2\alpha(\eta) + \epsilon_\parallel^e \sin^2\alpha(\eta)}. \tag{26}$$

Note that $\tilde{M}'(z)$ is independent of z *and, as a consequence, Eq. (14) can be solved analytically. The eigenvalues of* $\tilde{M}'$

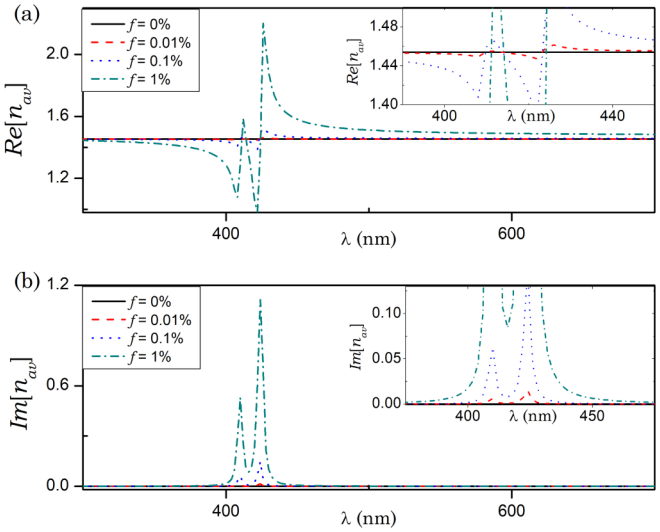

FIG. 3. Averaged refraction index $n_{av} = (n_1 + 2n_2)/3$ for an elastomer without deformation versus wavelength parametrized by the volume fraction f. (a) Real part and (b) imaginary part. In both panels, insets are shown.

are given by the secular equation $\mathrm{Det}(\tilde{M}' - k\tilde{I}) = 0$ *which is given explicitly by*

$$k^4 - k^2[\beta\epsilon_\perp^e\zeta + \beta\zeta\epsilon_d(\eta) + 2q^2] + \beta^2\epsilon_\perp^e\zeta^2\epsilon_d(\eta) - \beta\epsilon_\perp^e\zeta q^2 + q^4 - \beta\zeta q^2\epsilon_d(\eta) = 0 \quad (27)$$

and whose different solutions are

$$k_{1,2}^2 \equiv q^2 + \tfrac{1}{2}[\epsilon_d(\eta) + \epsilon_\perp^e]\zeta\beta \mp \frac{1}{2}\sqrt{\zeta\beta\{8q^2[\epsilon_d(\eta) + \epsilon_\perp^e] + \zeta\beta[\epsilon_\perp^e - \epsilon_d(\eta)]^2\}}. \quad (28)$$

In the case when there are no inclusions, $f = 0$, hence there exists a region of wavelengths where k_1 is purely imaginary and the propagation of electromagnetic waves is not allowed. This *interval is defined by the positive roots of the equation*

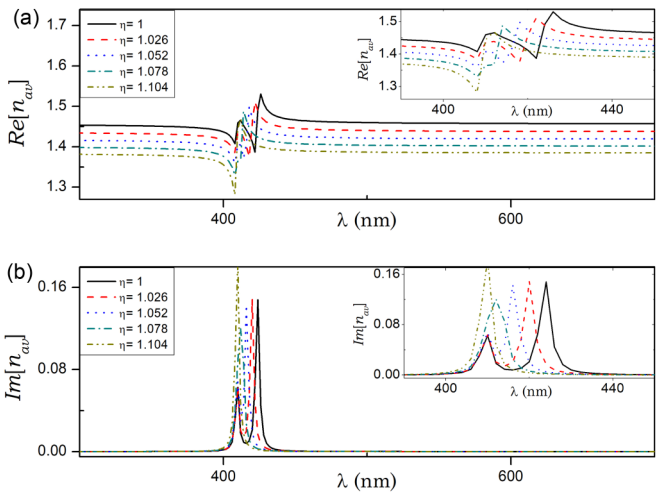

FIG. 4. The same as Fig. 3 but parametrized by the deformation parameter η for the volume fraction $f = 0.001$. (a) Real part and (b) imaginary part. In both panels, insets are shown.

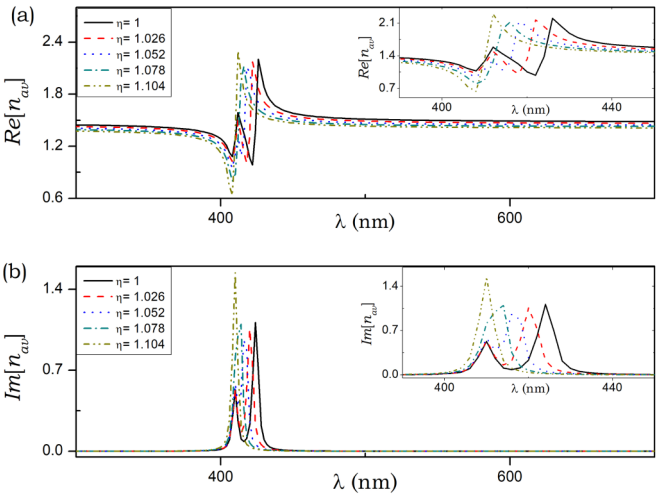

FIG. 5. The same as Fig. 4 but parametrized by the deformation parameter η for the volume fraction $f = 0.01$. (a) Real part and (b) imaginary part. In both panels, insets are shown.

$k_1^2 = 0$ *whose corresponding wavelengths are given by*

$$\lambda_1 \equiv \frac{2\pi\eta}{q_o c}\sqrt{\epsilon_d(\eta)},\ \lambda_2 \equiv \frac{2\pi\eta}{q_o c}\sqrt{\epsilon_\perp^e}, \quad (29)$$

where $c = (\mu_0\epsilon_o)^{-1/2}$. *In this interval,* $k_1^{\pm}$ *are pure imaginary and their corresponding eigenvectors are linearly polarized.*

Notice that the eigenvalue k_2 is purely real for any value of λ. As mentioned above, the interval of wavelengths $\lambda_1 \leqslant \lambda \leqslant \lambda_2$ is known as the Bragg reflection regime where

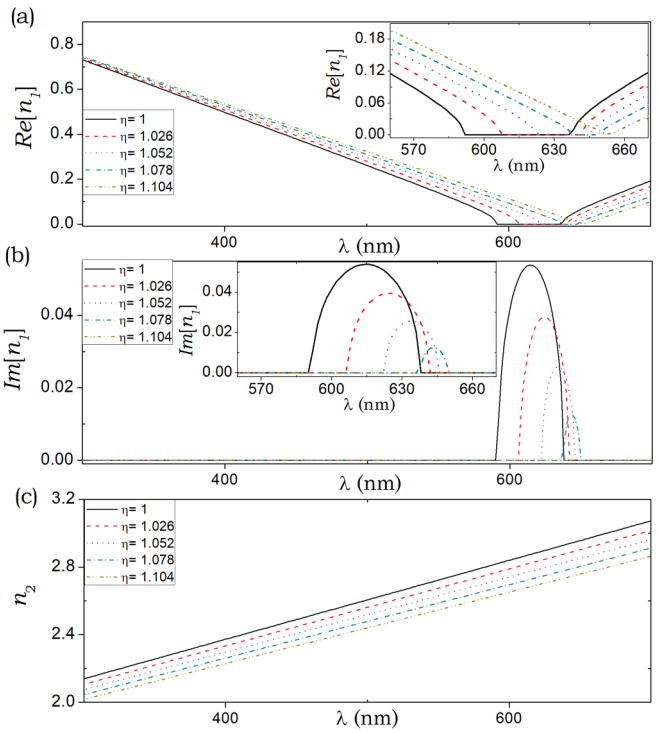

FIG. 6. Refraction indexes n_1 and n_2 for the elastomer without contamination ($f = 0$) against wavelength parametrized by η. (a) Real part of n_1, (b) imaginary part of n_1, and (c) real part of n_2.

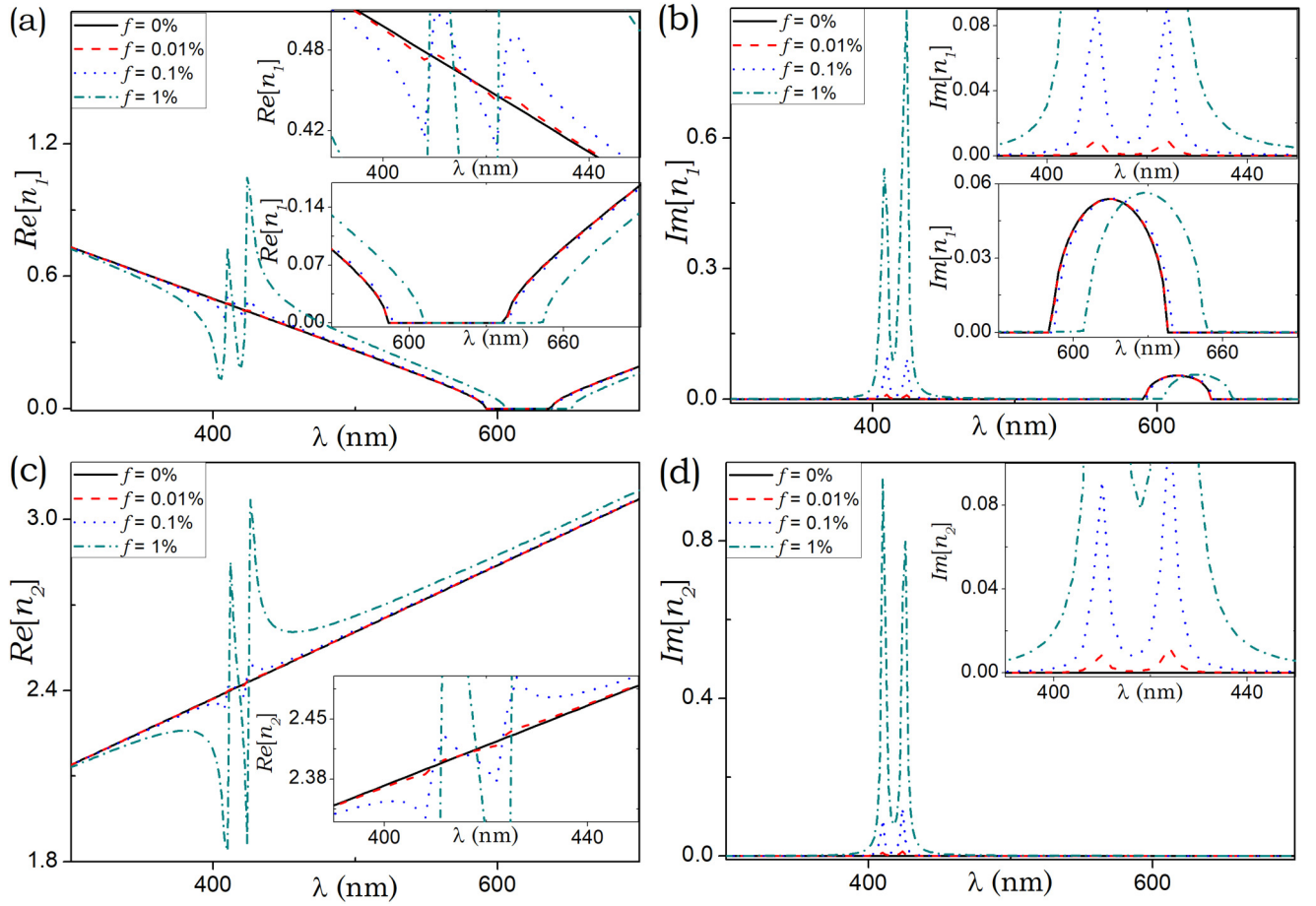

FIG. 7. Refraction indexes for a doped elastomer without deformation ($\eta = 1$) parametrized by f. (a) Real part of n_1, (b) imaginary part of n_1, (c) real part of n_2, and (d) imaginary part of n_2.

circularly polarized plane waves with the same handedness as the structural handedness are not allowed to propagate through the material. This prohibition is not present when a circularly polarized plane wave of the contrary handedness is incident [2]. In Ref. [31], the optical band gap of a liquid crystal cholesteric elastomer without inclusions is controlled by elongating the sample. It was found that a circular-polarization-filtering band gap is closed when elastomer is stretched. In this paper we analyze the properties of such a band gap but for a doped cholesteric elastomer, that is under the influence of small inclusions in the sample for different small filling factors.

It is worth to remark that, in the general case for $f > 0$, due to the resonant properties of the relative permittivity tensor, when the resonant wavelength lies inside the band gap, there will be significant changes in band structure with respect to the system without inclusions. Also, we notice that the condition $k_1 = 0$ will provide multiple band edges due to the complex dependence of the permittivities on λ. Moreover in addition, k_2 will no longer be purely real for any value of λ.

D. Reflection and transmission

By virtue of linearity, the solution of the 4×4 matrix ordinary differential equation (24) must be of the form

$$\mathbf{v}(z_2) = \tilde{U}(z_2 - z_1) \cdot \mathbf{v}(z_1)\,. \tag{30}$$

With $z_1 = 0$, the matrix $\tilde{U}(L)$ may be computed using the piecewise homogeneity approximation method [4].

The procedure to obtain the unknown reflection and transmission amplitudes thus involves the 4×4 matrix relation

$$\mathbf{f}_{\text{exit}} = \tilde{U}(L) \cdot \mathbf{f}_{\text{entry}}, \tag{31}$$

where the column 4 vectors

$$\mathbf{f}_{\text{entry}} = \frac{1}{\sqrt{2}} \begin{pmatrix} (r_L + r_R) + (a_L + a_R) \\ i[-(r_L - r_R) + (a_L - a_R)] \\ -i[(r_L - r_R) + (a_L - a_R)]/\eta_o \\ -[(r_L + r_R) - (a_L + a_R)]/\eta_o \end{pmatrix} \tag{32}$$

and

$$\mathbf{f}_{\text{exit}} = \frac{1}{\sqrt{2}} \begin{pmatrix} t_R + t_R \\ i\,(t_R - t_R) \\ -i(t_R - t_R)/\eta_o \\ (t_R + t_R)/\eta_o \end{pmatrix} \tag{33}$$

contain $\eta_o = \sqrt{\mu_o/\epsilon_o}$ as the intrinsic impedance of free space.

The reflection amplitudes $r_{L,R}$ and the transmission amplitudes $t_{L,R}$ can be computed for specified incident amplitudes (a_L and a_R) by solving (31). Interest usually lies in determining the reflection and transmission coefficients entering the 2×2

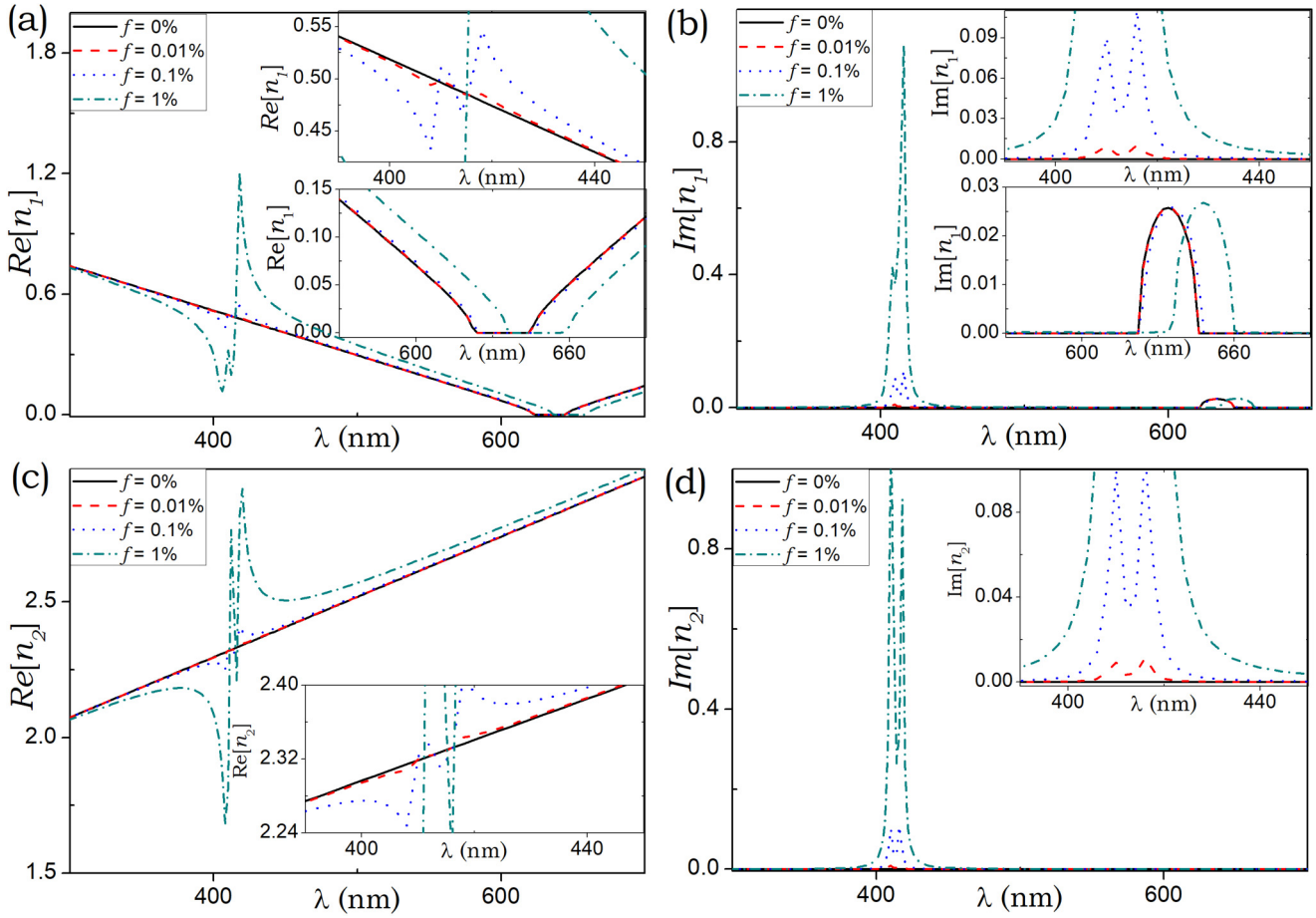

FIG. 8. Refraction indexes for a doped stretch elastomer ($\eta = 1.054$) parametrized by f. (a) Real part of n_1, (b) imaginary part of n_1, (c) real part of n_2, and (d) imaginary part of n_2.

matrices in the following two relations:

$$\begin{pmatrix} r_L \\ r_R \end{pmatrix} = \begin{pmatrix} r_{LL} & r_{LR} \\ r_{RL} & r_{RR} \end{pmatrix} \begin{pmatrix} a_L \\ a_R \end{pmatrix}, \tag{34}$$

$$\begin{pmatrix} t_R \\ t_R \end{pmatrix} = \begin{pmatrix} t_{LL} & t_{LR} \\ t_{RL} & t_{RR} \end{pmatrix} \begin{pmatrix} a_L \\ a_R \end{pmatrix}. \tag{35}$$

Both 2×2 matrices are defined phenomenologically. The copolarized transmission coefficients are denoted by t_{LL} and t_{RR}, and the cross polarized ones by t_{LR} and t_{RL}, and similarly for the reflection coefficients. Reflectances and transmittances are denoted, e.g., as $T_{LR} = |t_{LR}|^2$.

IV. RESULTS AND DISCUSSION

Hitherto we restrict our calculations for particular host and guest materials of the kind we have discussed above. The cholesteric elastomer parameters we use for our calculations are $r = 1.16$, $L = 8.56\ \mu$m, $\frac{p}{2} = 214$ nm, $\epsilon_\perp = 1.91$, $\epsilon_\parallel = 2.22$, $\mu = 1$ which correspond to a real sample made by a siloxane backbone chain reacting with 90 mol % and 10% of the flexible difunctional cross-linking groups (di-11UB). The rodlike mesogenic groups are present in the proportion 4:1 between the nematic 4-pentylphenyl-4'- (4-buteneoxy) benzoate (PBB) and the derivative of chiral cholesterol pentenoate (ChP) [32]. Finally, we take silver nanospheres $\epsilon_0 = 5$, $\omega_p = 1.367 \times 10^{16}$ Hz, and $\gamma = 3.03 \times 10^{13}$ Hz.

As a starting point of this section, we examine certain aspects concerning the dielectric resonance of the whole nanocomposite structure. For this purpose, in Figs. 3–5 we plot the real and imaginary parts of the average refractive index n_{av}, which is defined as [33]

$$n_{av}(\lambda) = \left(\sqrt{\epsilon_\perp^e(\lambda)} + 2\sqrt{\epsilon_d(\eta,\lambda)}\right)/3, \tag{36}$$

for several filling fractions. Here, $\epsilon_\perp^e(\lambda)$ and $\epsilon_d(\eta,\lambda)$ are given by expressions (17) and (26), respectively.

In Fig. 3 we have depicted the case of an undeformed elastomer as function of the wavelength. It can be evidently observed in Fig. 3(a) for Re[n_{av}], that the inclusion of metallic nanoparticles into the chiral medium provokes the appearance of two optical resonances which are contained in the interval (350 and 500 nm). The magnitude of the resonances increase and their peaks displace towards longer wavelengths as the filling factor gets larger. Complementarily, Fig. 3(b) for Im[n_{av}] show two maxima of absorptions whose magnitude depends strongly on the filling factor.

We should mention that $n_{av}(\lambda)$ is independent of the wavelength when there is no contamination in the elastomer, but it still depends on the stretching factor. In contrast, when the filling factor is not vanishing but small ($f = 0.001$) Re[$n_{av}(\lambda)$], as it displayed in Fig. 4(a), exhibits two maxima

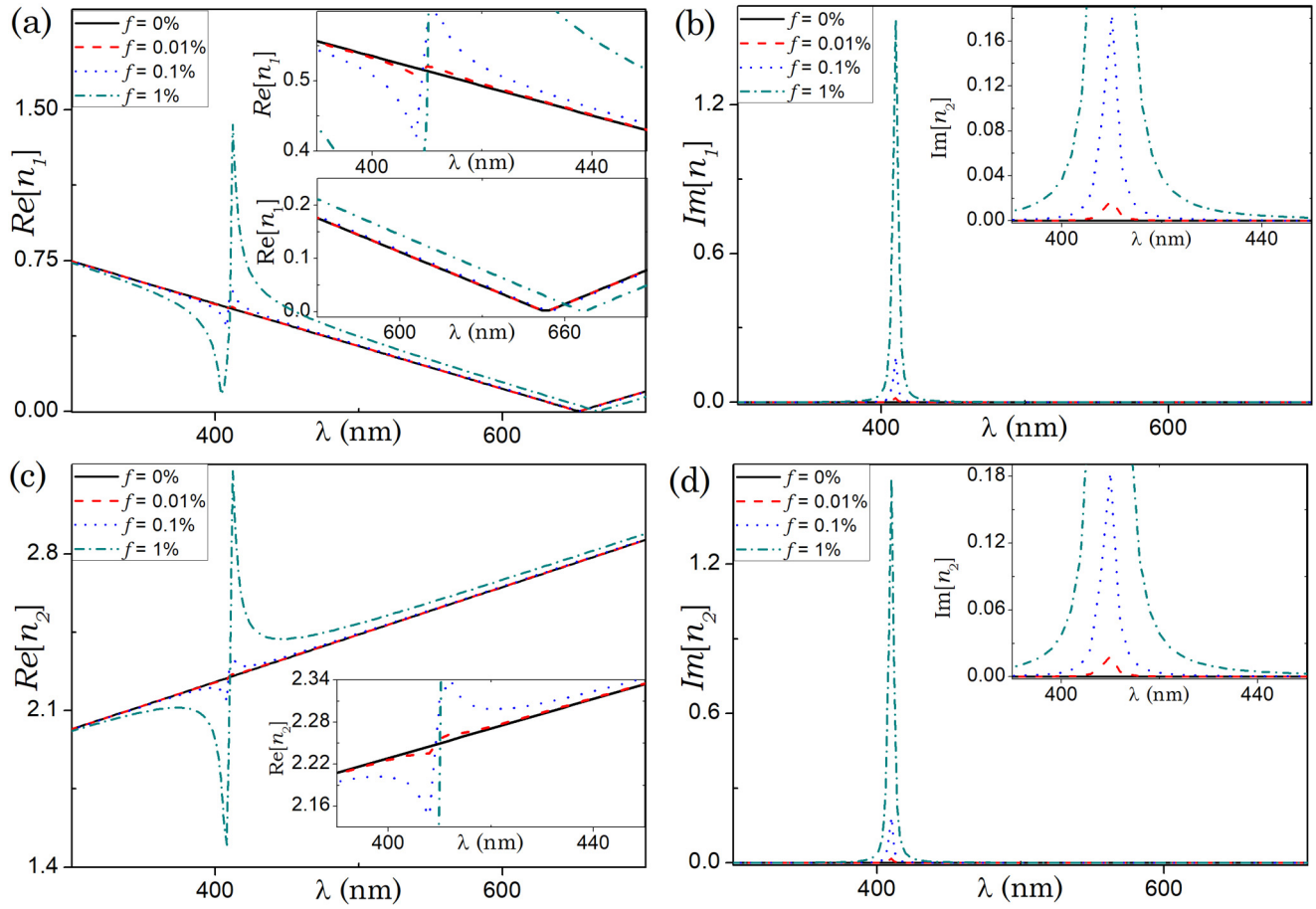

FIG. 9. Refraction indexes for a doped stretch elastomer ($\eta = 1.104$) parametrized by f. (a) Real part of n_1, (b) imaginary part of n_1, (c) real part of n_2, and (d) imaginary part of n_2.

and minima versus wavelength which red-shifts when the elastomer stretches. Additionally, in Fig. 4(b) $\mathrm{Im}[n_{av}(\lambda)]$ shows various absorption maxima as a function of wavelength which changes from two to the one in the shortest wavelength, as the elastomer is stretched.

We have depicted in Figs. 5(a) also $n_{av}(\lambda)$ but for a larger filling factor (0.01). In this case, the maxima of the curves of Fig. 5(a) get larger almost by an order of magnitude in comparison with Fig. 4(a) whereas the relative differences among the curves corresponding to the various stretch are less remarkable than in Fig. 4(a). Also Fig. 5(b) shows a similar behavior as Fig. 4(b) but in this case the respective absorption peaks are consistently much larger.

We have plotted separately in Fig. 6 the refraction indexes n_1 and n_2 for the elastomer without contamination ($f = 0$) versus the wavelength parametrized by η. Figure 6(a) for $\mathrm{Re}[n_1]$ presents explicitly the typical reflection band of a cholesteric which for this material is delimited to the interval (592 and 636 nm) when the sample is not deformed. Nevertheless, when the elastomer is stretched the lower band edge displaces until the band reflection get closed as was already reported in Ref. [31]. Figures 6(b) and 6(c) present $\mathrm{Im}[n_1]$ and n_2 which also have the usual profile for cholesterics, in which the first one has a semicircle form starting in one band edge and finishing in the other, whereas n_2 does not have any band reflection.

In Fig. 7, we have depicted the real and imaginary parts of both refraction indexes n_1 and n_2 versus the wavelength of an undeformed elastomer ($\eta = 1$) parametrized by the filling factor f. Figure 7(a) for $\mathrm{Re}[n_1]$ exhibits how both edges of the band reflection greatly red-shifts as the filling factor increases. Indeed, these edges displace about a quarter of the whole bandwidth when the filling factor changes from 0 to 1% as it is also shown in the bottom inset. Alternatively, we can express this red-shift as the average of 1300 nm per unit of volume fraction (UVF) for silver nanospheres which is of the same order as the red-shift found by Lakhtakia [19] in silver doped chiral sculptured thin films.

Besides, in the top inset it is displayed a region in the near infrared where oscillations of $\mathrm{Re}[n_1]$ emerge whose amplitude grow with f. On the other hand, Fig. 7(b) corresponding to $\mathrm{Im}[n_1]$ shows how the absorption in the top inset and the evanescence in the bottom inset vary with the filling factor. The amplitude of the first one increases whereas the position of the second red-shifts as f gets larger. The second refraction index n_2 is also influenced by the presence of the inclusion as it is evidenced in Fig. 7(c) for $\mathrm{Re}[n_2]$ which oscillates stronger against wavelength as f grows. Figure 7(d)

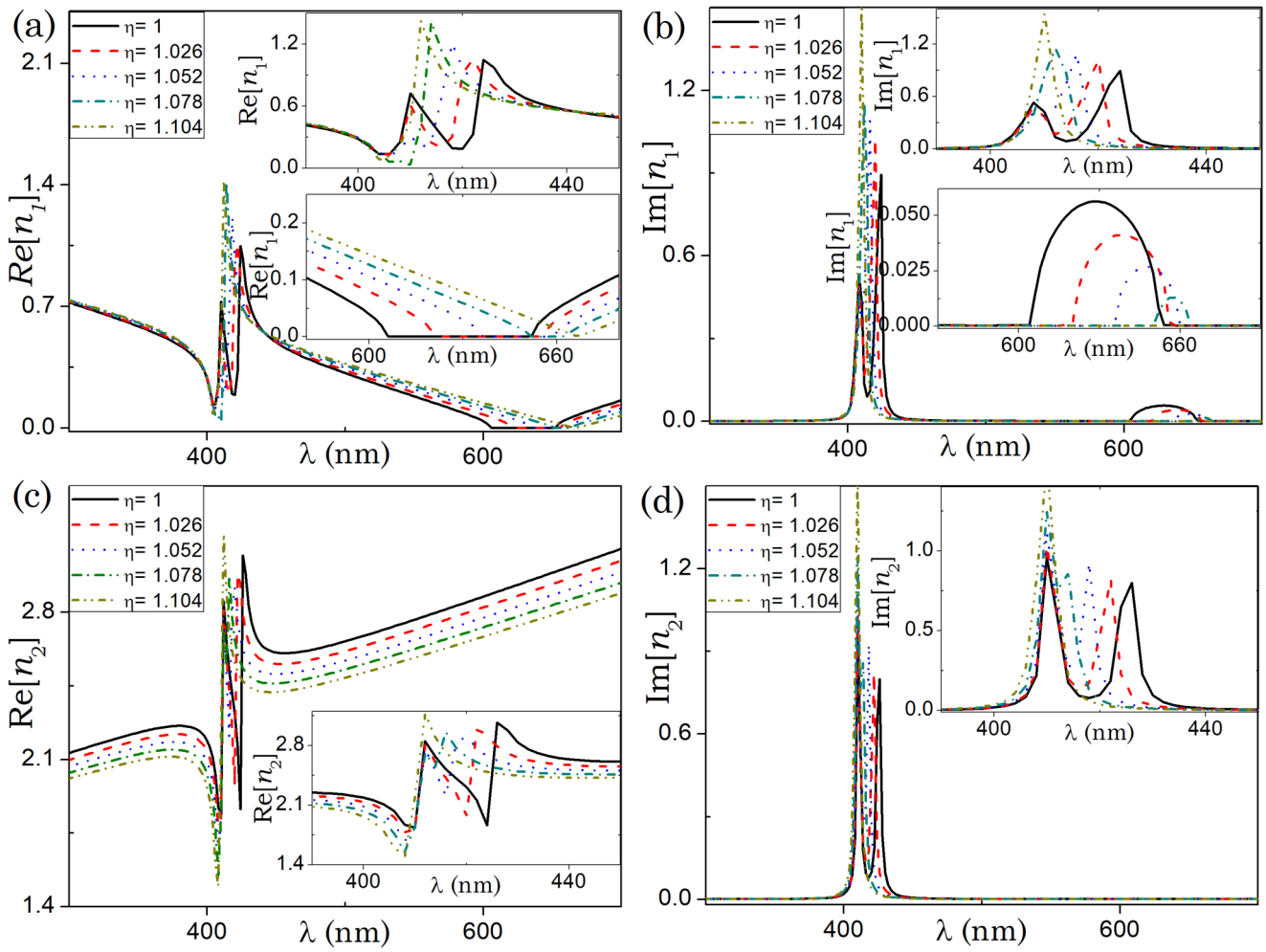

FIG. 10. Refraction indexes for a doped stretch elastomer ($f = 0.01$) parametrized by the deformation parameter η. (a) Real part of n_1, (b) imaginary part of n_1, (c) real part of n_2 and (d) imaginary part of n_2.

for Im[n_2] presents two peaks of absorption induced by the particulate nanospheres.

We have plotted in Fig. 8 the refraction indexes corresponding to a partially stretched elastomer when the deformation parameter is $\eta = 1.054$. The two featuring intervals, that is the reflection band and the oscillating region obtained without deformation in Fig. 7, are also found for this case. However, their positions are translated to other wavelengths. In general the same characteristic of Fig. 7 is shared by Fig. 8.

In Fig. 9 we have depicted the refraction indexes of a complete stretched elastomer. Under these circumstances, the reflection band in Fig. 9(a) has been completely closed in such way it has turned out into a single point of the band structure. Consistently, Fig. 9(b) for Im[n_1] only displays a unique absorption peak associated with the metallic resonance. Figures 9(c) and 9(d) for n_2 have the oscillations corresponding to the same metallic resonance.

In Fig. 10 the refraction indexes for a doped stretched elastomer ($f = 0.01$) are parametrized by the deformation parameter η instead of the filling factor. This plot allows to observe how the changes induced by the contamination are larger than those generated by the elastomer deformation even though the stretching is able to close the band reflection. For this small value of f, the oscillation caused by the metallic resonance is not so large. The absorption peaks of Fig. 10(d) and the absorption and evanescence peaks of Fig. 10(b) are congruously present.

It is also worth to mention that in all the plots for the real part of the diffraction indexes analyzed, there are various wavelength intervals for which the slopes of the curves are negative which correspond to region where the group is negative as well $d\omega/dk < 0$. In these regions, the Poynting vector is antiparallel to the wave vector which is a feature characterizing the behavior of a metamaterial which in some sense is to be expected because the helical geometry of the cholesteric resembles some of the structure proposed in the literature for metamaterials.

In Fig. 11 reflectance (R_{RR}, R_{LR}, and R_{LL}) and transmittance (T_{RR}, T_{LR}, and T_{LL}) spectra as function of the wavelength, corresponding to a slab of metal doped elastomer cholesteric of 22 periods made with the same materials considered for the other plots. We have taken a filling factor $f = 0.01$, with $\eta = 1$ for (a) and (b) while $\eta = 1.05$ for (c) and (d). In the right panel of Fig. 11(a) two peaks are shown for R_{RR}, R_{LL} where the second one is twice larger than the first one, while R_{LR} show also both peaks which are four times

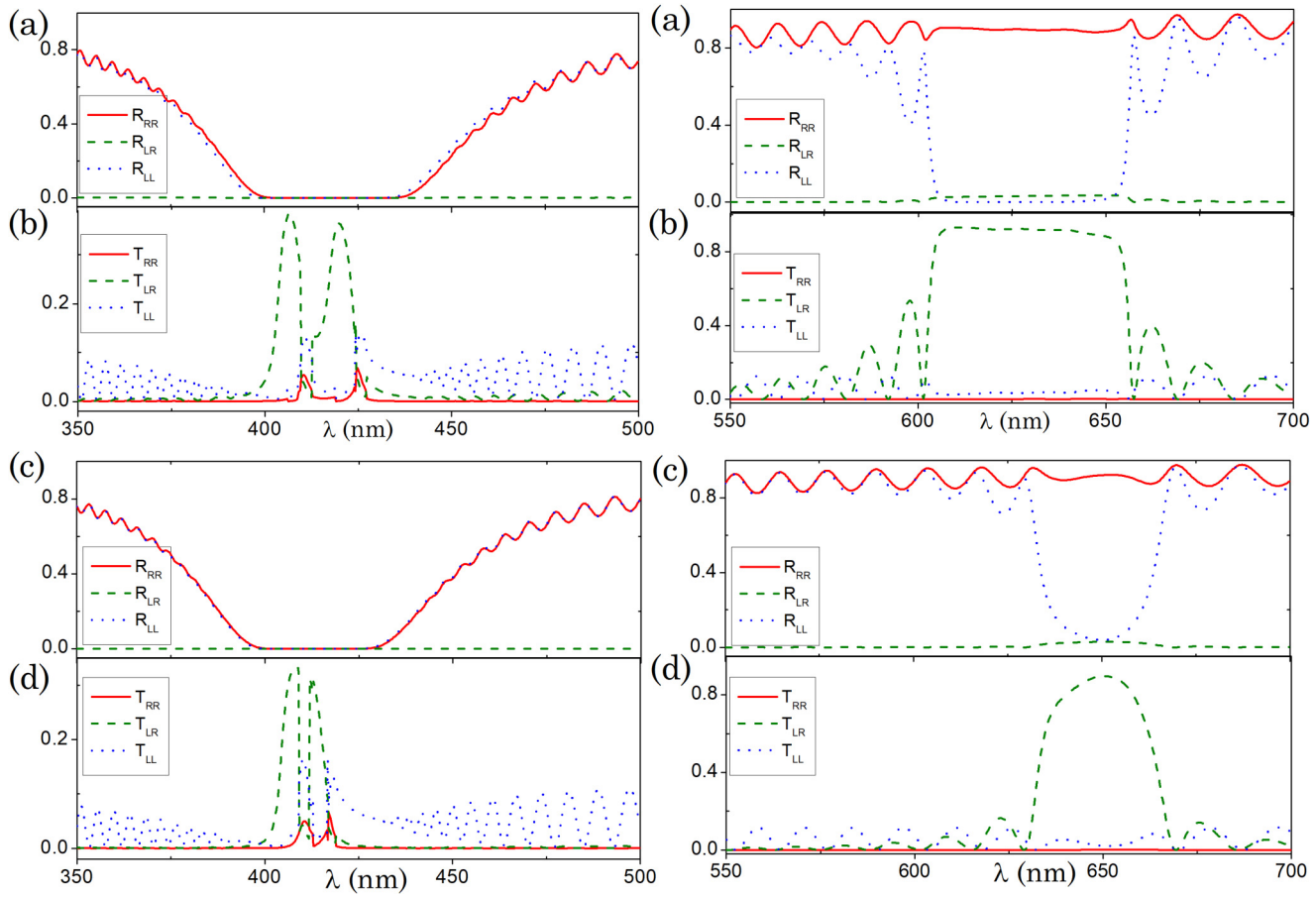

FIG. 11. Reflectance (R_{RR}, R_{LR}, and R_{LL}) and transmittance (T_{RR}, T_{LR}, and T_{LL}) versus vacuum wavelength for $f = 0.01$, in (a) and (b) $\eta = 1$ and in (c) and (d) $\eta = 1.05$. The right panels display the interval (350 nm, 500 nm) whereas the left panels show the interval (550 nm, 700 nm).

larger and their positions are red-shifted. Figure 11(b) presents essentially the same reflection band for the three polarized and copolarized transmittances. Figure 11(d) exhibits the same two peaks but they are nearer when the elastomer is stretched. The right panel of the same plots exhibits the highest wavelength interval which exhibit a typical spectrum for a cholesteric structure whose bandwidth is reduced by keeping its form when the elastomer is stretched ($\eta = 1.05$) as can be observed in Figs. 11(c) and 11(d).

V. CONCLUSIONS

We have studied the reflection band for axially propagating electromagnetic waves throughout a nanocomposite made with a cholesteric elastomer doped by silver nanospheres randomly, whose dielectric properties can be represented by a resonant effective uniaxial tensor. We have established the Maxwell equations in a 4×4 matrix representation. We have computed the eigenvectors and eigenvalues of the corresponding matrix in the system rotating along with the chiral structure for a specific sample. One of the eigenvalues showed wavelength intervals where a circularly polarized optical wave is not allowed to propagate. We have found that the band gap properties of the periodic system depends strongly on the volume fraction of nanoparticles in the chiral matrix, even for quite small values of the volume fraction. The cholesteric elastomer phase we use for our study is a sample made by a siloxane backbone chain reacting with 90 mol % and 10% of the flexible difunctional cross-linking groups (di-11UB). We have found that the center of the cholesteric band reflection displaces even until a quarter of the band width, when the volume fraction increases from 0 to 0.01. Also, the bandwidth decreases until it vanishes as the elastomer is gradually stretched. To confirm our results, we have calculated the transmittance and reflectance spectra for our system. These calculations are in agreement with the band structure findings. We hope that our research could promote the construction of this type of hybrid media.

ACKNOWLEDGMENT

J. A. Reyes acknowledges financial support from Grant No. DGAPA-PAPIIT IN110012-3.

[1] H. A. Macleod, *Thin-Film Optical Filters*, 3rd ed. (Institute of Physics Publishing, Bristol, 2001).

[2] P. G. de Gennes and J. Prost, *The Physics of Liquid Crystals*, 2nd ed. (Clarendon, Oxford, 1993), Chap. 6.

[3] C. G. Avendaño, S. Ponti, J. A. Reyes, and C. Oldano, J. Phys. A: Math. Gen. **38**, 8821 (2005).
[4] A. Lakhtakia and R. Messier, *Sculptured Thin Films: Nanoengineered Morphology and Optics* (SPIE, Bellingham, WA, 2005), Chap. 9.
[5] D. A. Pinnow, R. L. Abrams, J. F. Lotspeich, D. M. Henderson, T. K. Plant, R. R. Stephens, and C. M. Walker, Appl. Phys. Lett. **34**, 391 (1979).
[6] J. A. Reyes and A. Lakhtakia, Opt. Commun. **259**, 164 (2006).
[7] M. Warner and E. M. Terentjev, *Liquid Crystals Elastomers* (Clarendon, Oxford, 2003), Chap. 9.
[8] S. Kim and H. Finkelmann, Marcromol. Rapid Commun. **2**, 317 (1981).
[9] A. Komp, J. Rühe, and H. Finkelmann, Macromol. Rapid Commun. **26**, 813 (2005).
[10] J. Schmidtke, S. Kniesel, and H. Finkelmann, Macromolecules **38**, 1357 (2005).
[11] M. Rivera and J. A. Reyes, Appl. Phys. Lett. **90**, 023513 (2007).
[12] A. N. Oraevskii and I. E. Protsenko, JETP Lett. **72**, 445 (2000).
[13] S. Y. Vetrov, R. G. Bikbaev, and I. V. Timofeev, JETP **117**, 988 (2013).
[14] J. C. W. Lee and C. T. Chan, Opt. Express **13**, 8083 (2005); P. C. P. Hrudey, B. Szeto, and M. J. Brett, Appl. Phys. Lett. **88**, 251106 (2006); M. Thiel, M. Decker, M. Deubel, M. Wegener, S. Linden, and G. von Freymann, Adv. Mater. **19**, 207 (2007).
[15] A. Papakostas, A. Potts, D. M. Bagnall, S. L. Prosvirnin, H. J. Coles, and N. I. Zheludev, Phys. Rev. Lett. **90**, 107404 (2003); M. Kuwata-Gonokami, N. Saito, Y. Ino, M. Kauranen, K. Jefimovs, T. Vallius, J. Turunen, and Y. Svirko, *ibid.* **95**, 227401 (2005); E. Plum, V. A. Fedotov, A. S. Schwanecke, N. I. Zheludev, and Y. Chen, Appl. Phys. Lett. **90**, 223113 (2007); M. Thiel, G. von Freymann, and M. Wegener, Opt. Lett. **32**, 2547 (2007).
[16] A. V. Rogacheva, V. A. Fedotov, A. S. Schwanecke, and N. I. Zheludev, Phys. Rev. Lett. **97**, 177401 (2006); M. Decker, M. W. Klein, M. Wegener, and S. Linden, Opt. Lett. **32**, 856 (2007); E. Plum, J. Zhou, J. Dong, V. A. Fedotov, T. Koschny, C. M. Soukoulis, and N. I. Zheludev, Phys. Rev. B **79**, 035407 (2009).
[17] Y. Fan, Z. Wei, H. Li, H. Chen, and C. M. Soukoulis, Phys. Rev. B **88**, 241403(R) (2013).
[18] J. K. Gansel, M. Thiel, M. S. Rill, M. Decker, K. Bade, V. Saile, G. von Freymann, S. Linden, and M. Wegener, Science **325**, 1513 (2009).
[19] A. Lakhtakia, J. Nanophotonics **1**, 019502 (2007).
[20] S. Chandrasekhar, *Liquid Crystals* (Cambridge University Press, Cambridge, 1997).
[21] Y. Mao, E. M. Terentjev, and M. Warner, Phys. Rev. E **64**, 041803 (2001).
[22] N. Marcuvitz and J. Schwinger, J. Phys. D: Appl. Phys. **22**, 806 (1951).
[23] J. C. M. Garnett, Philos. Trans. R. Soc. London, Sect. A **3**, 385 (1904).
[24] M. Koledintseva, R. Dubroff, and R. Schwartz, Prog. Electromagn. Res. (PIER) **63**, 223 (2006).
[25] S. Y. Vetrov, A. Y. Avdeeva, and I. V. Timofeev, J. Exp. Theor. Phys. **113**, 755 (2011).
[26] A. Lakhtakia, B. Michel, and W. S. Weiglhofer, J. Phys. D: Appl. Phys. **30**, 230 (1997).
[27] A. Lakhtakia, Microsc. Opt. Tech. Lett. **11**, 290 (1996).
[28] T. G. Mackay and A. Lakhtakia, Opt. Commun. **234**, 35 (2004).
[29] T. G. Mackay, J. Nanophotonics **1**, 019501 (2007).
[30] C. W. Oseen, J. Chem. Soc. Faraday Trans. II **29**, 883 (1933).
[31] T. Espinosa-Ortega and J. A. Reyes, Opt. Commun. **281**, 5830 (2008).
[32] P. Cicuta, A. R. Tajbakhsh, and E. M. Terentjev, Phys. Rev. E **65**, 051704 (2002).
[33] J. Li, S. Gauza, and S.-T. Wu, J. Appl. Phys. **96**, 19 (2004).